Supplementary Information

Rego-Costa, A; Débarre, F; Chevin, LM. 2017. Chaos and the (un)predictability of evolution in a changing environment. *Evolution*.

Details of the model

We extend the evolutionary model in a constant environment by Doebeli & Ispolatov (2014) to a fluctuating environment. The model takes as a starting point logistic population growth where the strength of density dependence depends on phenotype-mediated interactions,

$$\frac{\partial N(\mathbf{y},t)}{\partial t} = rN(\mathbf{y},t)\left(1 - \frac{\int \alpha(\mathbf{y},\mathbf{x})N(\mathbf{x},t)d\mathbf{x}}{K(\mathbf{y})}\right), \tag{S1}$$

where $N(\mathbf{y},t)$ is the number of individuals of type $\mathbf{y}$ at time t. The phenotype of an individual is represented by a vector $\mathbf{x}$ (or $\mathbf{y}$) of length d, the number of traits under selection; d is called the dimensionality or complexity of the organism (Doebeli & Ispolatov, 2014). Interactions are mediated by phenotypes: an interaction kernel $\alpha(\mathbf{y},\mathbf{x})$ represents the fitness effects of interactions with individuals of phenotype $\mathbf{x}$ on individuals of phenotype $\mathbf{y}$. These interactions can either be positive (e.g. cooperation) or negative (e.g. competition) depending on the sign of α (negative and positive, respectively). The interaction kernel is standardized such that $\alpha(\mathbf{y},\mathbf{y}) = 1$ for all $\mathbf{y}$, but the exact form of the interaction kernel does not have to be specified at the moment. Another component of fitness is due to adaptation to the current environmental condition. It takes the form of a phenotype-dependent carrying capacity K, causing stabilizing selection towards a multivariate optimal phenotype θ. Specifically, we have

$$K(\mathbf{x}) = \exp\left(-\frac{1}{4}\sum_{i=1}^{d}(x_i - \theta_i)^4\right). \tag{S2}$$

We use a quartic function because it is the form assumed by Doebeli & Ispolatov (2014). A more general form could include weights for the different traits, and even interactions between the traits, but we want to stay close to their original model.

The size of the entire population is assumed to be large; reproduction is clonal; mutations are rare, and of small phenotypic effect. To study the evolution of the mean phenotype in the population, and to facilitate comparison of our results with those of Doebeli & Ispolatov (2014), we conform to their adaptive dynamics approach (also known as invasion analysis). Under this framework, the population is always fixed for a given phenotype, and evolution happens through a series of invasions of a population of resident phenotypes by better adapted mutants that differ by infinitesimally small phenotypic effects (Dieckmann & Law, 1996; Geritz *et al.*, 1998). Since mutations are assumed to be rare, population dynamics are faster than evolutionary dynamics, such that the population size equilibrates at the carrying capacity of the resident before any new mutant invades (in other words, ecological and evolutionary time scales are decoupled).

Using the adaptive dynamics assumptions above, Doebeli & Ispolatov (2014) demonstrate that the invasion fitness $f(\mathbf{y},\mathbf{x})$ of a mutant with phenotype $\mathbf{y}$ in a population fixed

for the resident phenotype $\mathbf{x}$, can be written as

$$f(\mathbf{y},\mathbf{x}) = 1 - \frac{\alpha(\mathbf{y},\mathbf{x})K(\mathbf{x})}{K(\mathbf{y})}\,. \tag{S3}$$

The rate and direction of evolutionary change at any time is then proportional to the selection gradient, i.e. the partial derivative of invasion fitness (*per capita* growth rate of a rare mutant) with respect to the invader's phenotype (Dieckmann & Law, 1996; Geritz *et al.*, 1998). If mutation effects are independent and of variance equal to one for all traits (which can be obtained by proper rescaling and change of coordinates, Martin & Lenormand, 2006; Doebeli & Ispolatov, 2014), the dynamics of evolution in the multidimensional phenotypic space depends solely on the multivariate selection gradient $\mathbf{s}(\mathbf{x}) = (s_1(\mathbf{x}), s_2(\mathbf{x}), \cdots, s_d(\mathbf{x}))$. Each component $s_i(\mathbf{x})$ of this vector is the partial derivative of the invasion fitness in equation (S3) relative to trait i of the mutant, evaluated at the resident phenotype for that trait, which leads to

$$s_i(\mathbf{x}) = \left.\frac{\partial f(\mathbf{y},\mathbf{x})}{\partial y_i}\right|_{\mathbf{y}=\mathbf{x}} = -\left.\frac{\partial \alpha(\mathbf{y},\mathbf{x})}{\partial y_i}\right|_{\mathbf{y}=\mathbf{x}} + \frac{\partial \ln[K(\mathbf{x})]}{\partial x_i}\,. \tag{S4}$$

Following Doebeli & Ispolatov (2014), we assume that the interaction kernel in equation (S3) is such that its derivative in equation (S4) is a quadratic function of phenotypes. Note that this implies that $\alpha(\mathbf{y},\mathbf{x})$ itself (rather than its derivative with respect to $\mathbf{y}$) is a third-order function of phenotypes, i.e. includes interactions between three traits, at least one of which belongs to the focal individual and one to its interactor. For simplicity, we do not consider interactions of even higher orders; including them would increase the likelihood of chaotic behavior due to the more complex feedbacks in the system (Ispolatov *et al.*, 2015).

A final important point about this model is that, if the interaction kernel depended only on the phenotypic difference between interactors rather than on their actual phenotypes, that is, if we had $\alpha(\mathbf{y},\mathbf{x}) = f(\mathbf{z})$ (where $\mathbf{z} = \mathbf{y} - \mathbf{x}$ and f is a function that does not involve $\mathbf{x}$ nor $\mathbf{y}$), then the corresponding term of the selection gradient in equation (S4) would be $f'(0)$, which is not a function of $\mathbf{z}$ and thus cannot be a function of $\mathbf{x}$ and $\mathbf{y}$. Hence the first two sums in eq. (1) in the main text would be null if $\alpha(\mathbf{y},\mathbf{x}) = f(\mathbf{y}-\mathbf{x})$, which would preclude the occurrence of chaotic dynamics, since stabilizing selection alone does not produce chaos in such a model.

The Lyapunov exponent

Chaotic dynamical systems can be identified by their Lyapunov exponents, which measure the rate of exponential increase in the distance between initially close trajectories in phenotype space (Ott, 2002). The main characteristic of chaotic systems is that, regardless of how close a set of trajectories start, trajectories initially diverge with time if they do not have the same exact initial state. Chaotic systems are, therefore, characterized by positive Lyapunov exponents (i.e. exponential rates of divergence). Dynamics that converge to cycles and fixed equilibrium states have zero and negative Lyapunov exponents, respectively. In multivariate systems, divergence can happen at different rates in different directions, but a positive rate of divergence in a single direction is sufficient for a system

to be chaotic. Therefore, knowledge of the largest Lyapunov exponents is sufficient to identify chaos.

We numerically estimate the largest Lyapunov exponents of all our simulated trajectories as described by Sprott (2001). Given a previously simulated trajectory $\{\mathbf{x}(0), \mathbf{x}(\mathrm{d}t), \mathbf{x}(2\mathrm{d}t), \cdots\}$, we start by picking a point $\mathbf{z}_0$ positioned in a random direction at a distance $\delta_0 = 10^{-3}$ from $\mathbf{x}(0)$. We then integrate the system from $\mathbf{z}_0$ for a single timestep $\mathrm{d}t$ the same way as done for the original trajectory. After this calculation, the distance δ_f between the reached point $\mathbf{z}_f$ and $\mathbf{x}(\mathrm{dt})$ is recorded. We finally reset point $\mathbf{z}_0$ to lie in the same direction that separates $\mathbf{z}_f$ and $\mathbf{x}(\mathrm{dt})$, at a distance $\delta_0 = 10^{-3}$ from $\mathbf{x}(\mathrm{dt})$, and proceed the integration from this point for another timestep. This process is iterated along the whole trajectory up to its end. The rate of divergence at each time step is calculated as

$$\lambda = \frac{1}{\mathrm{d}t} \ln\left(\frac{\delta_f}{\delta_0}\right). \tag{S5}$$

The estimate of the largest Lyapunov exponent is given by the asymptotic value of the average Lyapunov exponent as the number of considered time points tends to infinity, $\bar{\lambda}_\infty$. However, since we are interested in identifying transitions from chaotic to either periodic or equilibrium behavior, we used a local estimate of rates of divergence, $\bar{\lambda}(t)$, defined as the average λ in a window of 200 time units preceding time t (Supplementary Fig. S1). The length of this window was chosen such that there is enough smoothing of the short-term fluctuations of λ, while allowing for identification of transitions (as in Figure S1B). For simplicity, we refer to this measure in the main text as the Lyapunov exponent λ, omitting both the bar and t. Chaotic trajectories were easily distinguished from non-chaotic ones by visual inspection. Based on this criterion, we were able to categorize chaotic trajectories at a given time t if $\bar{\lambda}(t)$ was larger than a threshold $\mu = 0.05$ under a constant optimum, and $\mu = 0.02$ under an oscillating optimum. Trajectories were classified as converging to an equilibrium if $\bar{\lambda}(t) < -\mu$, or to a periodic cycle if $\left|\bar{\lambda}(t)\right| < \mu$.

References

Dieckmann, U. & Law, R. (1996). The dynamical theory of coevolution: a derivation from stochastic ecological processes. *Journal of mathematical biology*, 34, 579–612.

Doebeli, M. & Ispolatov, I. (2014). Chaos and unpredictability in evolution. *Evolution*, 68, 1365–1373.

Geritz, S., Kisdi, E., Meszéna, G. & Metz, J. (1998). Evolutionarily singular strategies and the adaptive growth and branching of the evolutionary tree. *Evolutionary Ecology*, 12, 35–57.

Ispolatov, I., Madhok, V., Allende, S. & Doebeli, M. (2015). Chaos in high-dimensional dissipative dynamical systems. *Scientific reports*, 5, 12506.

Martin, G. & Lenormand, T. (2006). A general multivariate extension of Fisher's geometrical model and the distribution of mutation fitness effects across species. *Evolution; international journal of organic evolution*, 60, 893–907.

Ott, E. (2002). *Chaos in Dynamical Systems*. 2nd edn.

Sprott, J.C. (2001). *Chaos and Time-Series Analysis*. Oxford University Press, Oxford.

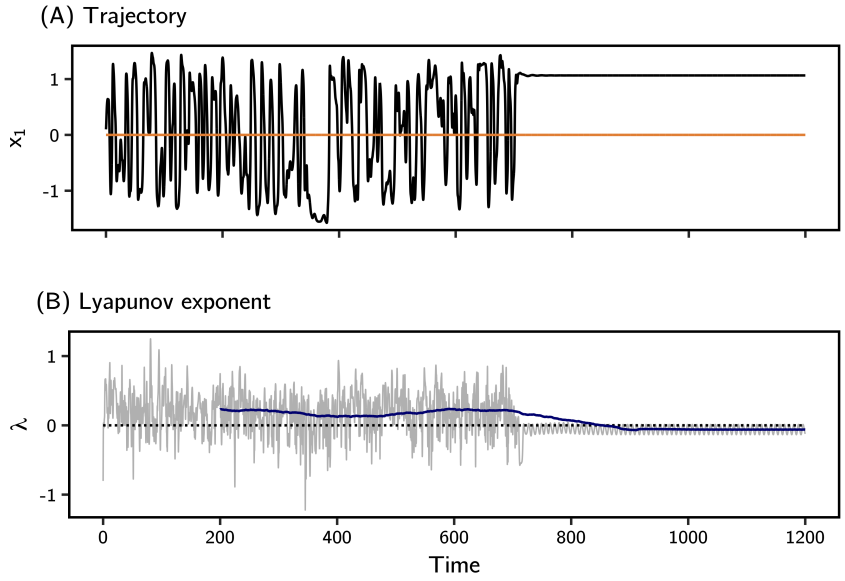

Fig. S1. Calculation of the window-averaged Lyapunov exponent $\bar{\lambda}(t)$. (A) The evolutionary trajectory for one single trait in a system of $d = 70$ is represented in black, under a constant optimum (orange). The dynamics transitions from chaos to a fixed point around time $t = 700$. (B) The Lyapunov exponent computed at each time point with equation (S5) varies substantially (gray line). However, when averaged over a window of 200 time units (in blue; calculated as described in the supporting text), the transition from chaos ($\lambda > 0$) to a fixed equilibrium ($\lambda < 0$) can be identified with some time lag.

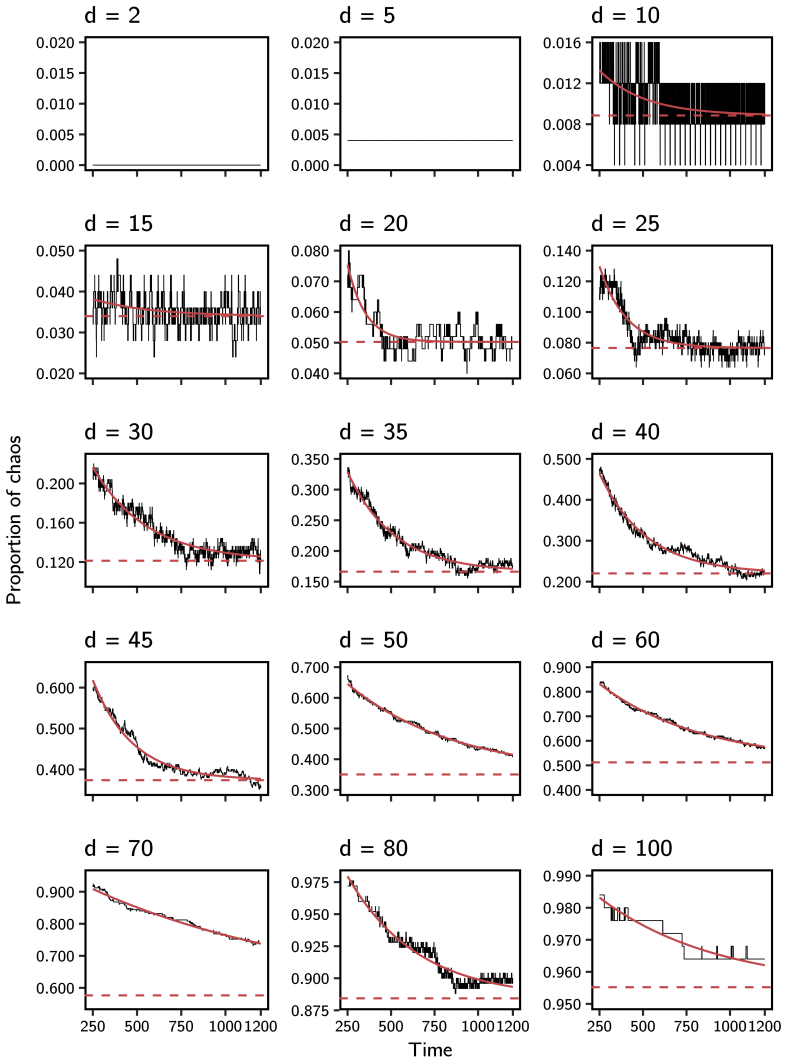

Fig. S2. The proportion of trajectories categorized as chaotic (according to their window-averaged Lyapunov exponent $\bar{\lambda}(t)$), out of 250 simulations under a constant optimum, decreases with time as some of them transition to either periodic cycles or fixed equilibria. Models of exponential decrease (red solid lines) were fit to the observed frequencies (as described in the Methods), and used to predict the asymptotic proportion of truly chaotic trajectories in infinite time (red dashed lines). Models were not fitted to dimensionalities $d = 2$ and 5 because of their insufficient number of chaotic trajectories. The black line in $d = 5$ is flat because the single chaotic trajectory observed did not transition during the simulation. The black lines in the other panels are jagged because the $\bar{\lambda}(t)$ of individual trajectories are only estimates that can switch between chaos and non-chaos in time.

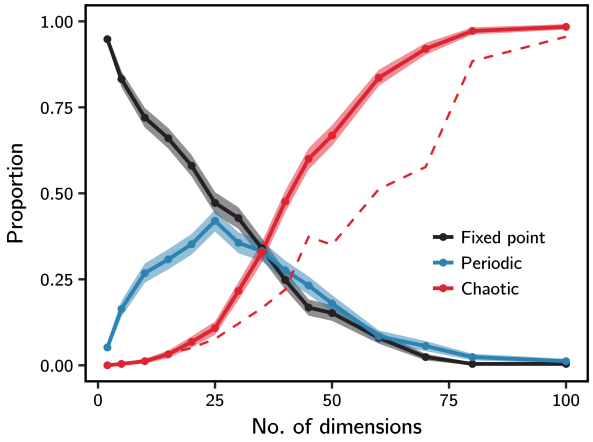

Fig. S3. Organismal complexity and the probability of (transient) chaos in a constant environment. The proportion of trajectories identified as fixed point, periodic or chaotic at the beginning of the simulations (classified by their $\bar{\lambda}(250)$) is represented in solid lines, with the standard errors of binomial proportions shown as shading. The proportion of trajectories identified as chaotic decreases with time, as transiently chaotic trajectories reach their eventual equilibrium fixed point or limit cycle. The red dashed line shows the asymptotic proportion of chaotic trajectories (at infinite time), as estimated from the exponential decrease, over $t = 1200$ time units, of the proportion of trajectories identified as chaotic (as described in the Methods and shown in Figure S2). Note that this curve is more noisy than the others, owing to error in estimation of the asymptotic values represented in Fig. S2. For each explored value of dimensionality d, estimations of frequencies of each type of dynamics were made based on 250 trajectories that were run up to $t = 1200$, as described in the main text.

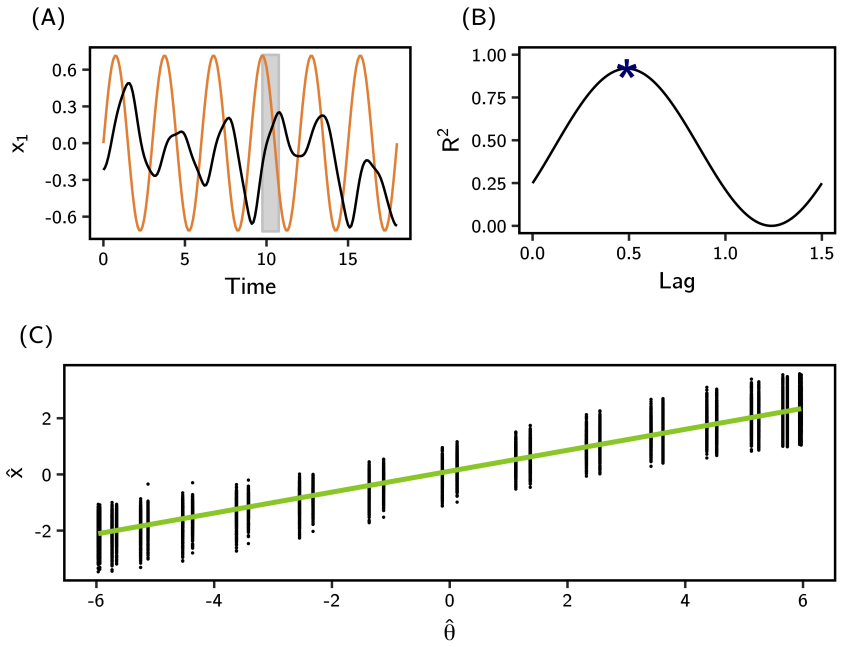

Fig. S4. Correction of phenotypic lag in the regression of the phenotype on the optimum. (A) Even for a chaotic evolutionary trajectory (black line), part of the variation is caused by tracking of the optimal phenotype that moves in response to the oscillating optimum (orange line). This tracking happens with a certain temporal lag (represented by the shaded interval). (B) By regressing the phenotype $\hat{x}_t$ at time t on the optimum $\hat{\theta}_{t-\tau}$ at an earlier time $t-\tau$ (both projected on the direction of environmental change in the optimum), the lag can be estimated by maximizing the R^2 of the regression (marked with a star) with respect to τ, over half a period of optimum oscillation. (C) The relationship between $\hat{x}_t$ and $\hat{\theta}_{t-\tau}$ corrected by the lag is represented for simulated values (dots), together with the corresponding regression line shown in green. The slope of this line is expected to equal the ratio between the amplitude of the tracking component of phenotype and that of the oscillating optimum.

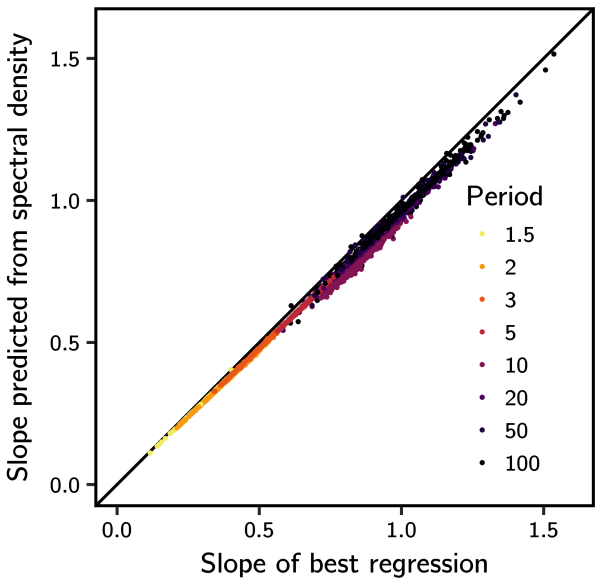

Fig. S5. Estimating the regression slope from the spectral density. On the x-axis, the regression slope of the phenotype on the optimum (after correction for the lag, as explained in Figure S4) is expected to approximate the ratio between the amplitudes of the tracking component of the phenotype, identified by the linear regression model, and the amplitude of optimum oscillation (as shown in Figure S4C). In the spectral analysis of the phenotypic time series, the peak spectral density can be used to identify the period of the tracking component, which equals that of the oscillating phenotype (as shown in Figure 3C and D). Given that the spectral density at any period equals half the squared amplitude of the trajectory's oscillation at that period, the amplitude of the tracking component of the trajectories can be estimated from this peak spectral density—as well as the ratio between this amplitude and that of the oscillating optimum. Here we show that this estimation, done for each trajectory independently (points, colored according to the period of optimum oscillation), closely approximates the slope of the regression models. However, this is only possible by interpolating the time-series of phenotype to increase the number of data points and, thus, improve the estimation of the spectral density at the period of optimum oscillation as done by the Fast-Fourier algorithm used here (as described in the Methods). We have made several of these estimations, each time linear-interpolating the time-series to a larger number of timepoints, one extra timepoint at a time up to the double of the original number of points. For each of these interpolated time-series, the peak spectral density was calculated, and the largest of these values (among all interpolated time-series of a single trajectory) was selected to estimate the amplitude of the component of phenotypic evolution that tracks the moving optimum.

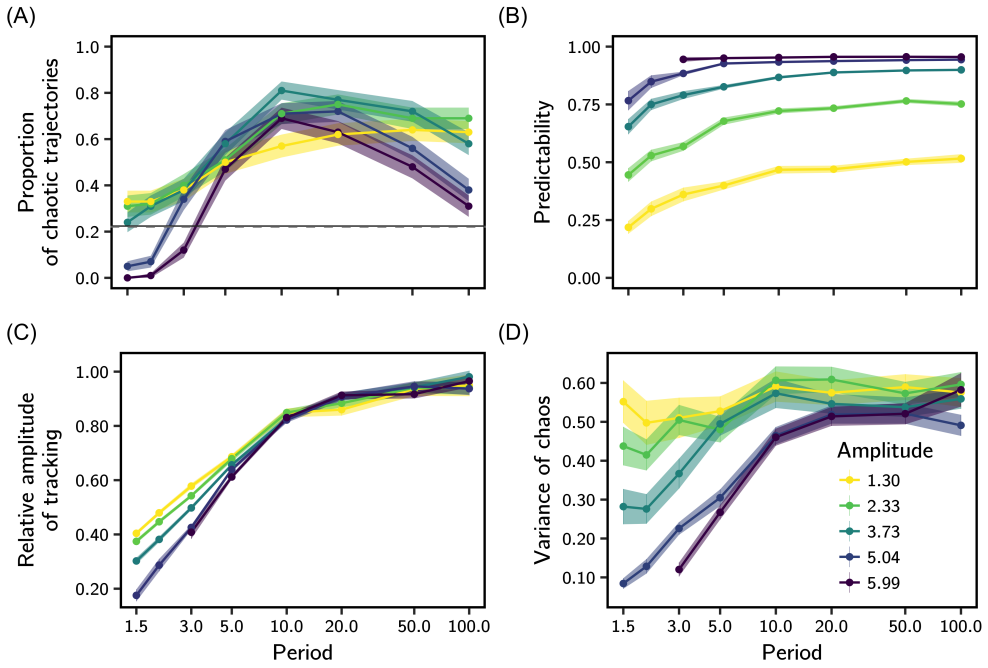

Fig. S6. Predictability of evolution in a system of lower dimensionality. Here we replicate the oscillating optimum analyses presented in the main text, but for systems of $d = 40$. (A) Similarly to results for $d = 70$, the proportion of trajectories that are chaotic is decreased in relation to that of constant environment for conditions of short periods and large amplitudes of oscillation (complete loss of chaos even occurred for amplitude 5.99 and periods 1.5 and 2). This proportion increased for longer periods as for $d = 70$, but this increase was not monotonic (compare with Figure 2 of the main text). Results for (B) the predictability of chaotic dynamics, (C) relative amplitude of tracking, and (D) variance of chaos, are qualitatively similar to those for $d = 70$. The dashed lines in A have the same meaning as in Figure 2, and the variables represented in B-D are defined as in Figure 4. We show the average (lines and points) and standard error (shading) over 100 simulations for each combination of amplitude and period of optimum oscillation. The 100 sets of interaction coefficients and initial phenotypes used here were taken arbitrarily from the 250 sets used in constant environment simulations for the same dimensionality.

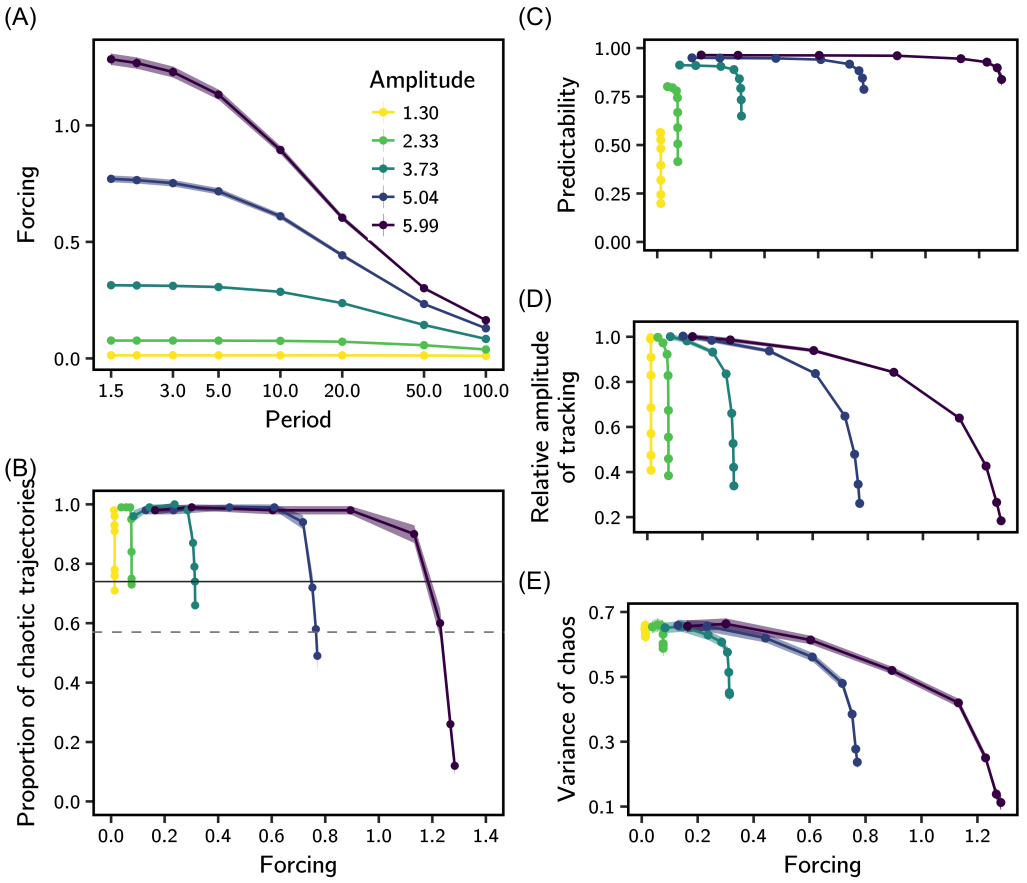

Fig. S7. Effect of the strength of environmental forcing. We used a version of the model without frequency-dependent selection (interaction coefficients b_{ij} and a_{ijk} were set to zero) to measure how different patterns of optimum oscillation translate into intensities of environmental forcing on the system. Under frequency-independent selection, the evolutionary dynamics are led exclusively by the rightmost term in equation (S4). We defined forcing as $|\hat{s}_i(x)|$, i.e. the absolute value of the scalar projection of the selection gradient in equation (S4) on the direction of environmental change (the diagonal of the phenotype space). This effectively measures the average magnitude of the selection pressure to which trajectories are submitted by the moving optimum. We solved the evolutionary dynamics numerically (as done in simulations with frequency dependence) until time $t = 200$, and computed the average forcing that trajectories experienced under the combinations of amplitudes and periods of optimum oscillation described in the main text. (A) A combination of short periods and large amplitudes of oscillation leads to the strongest forcing scenario. To assess whether this measure of forcing can partly explain our results *with* frequency-dependent selection, we plotted against it (B) the decrease in proportion of chaos (relative to a constant environment), (C) the predictability of evolutionary dynamics, (D) the relative amplitude of tracking, and (E) the variance of chaos. The dashed lines in B are the same as in Figure 2, and the variables represented in C-E are defined as in Figure 4. Each point represent the results for a single combination of amplitude and period of optimum oscillation. Points are colored by their respective amplitudes. We show the average (lines and points) and standard error (shading) over 100 simulations for each combination of amplitude and period of optimum oscillation.

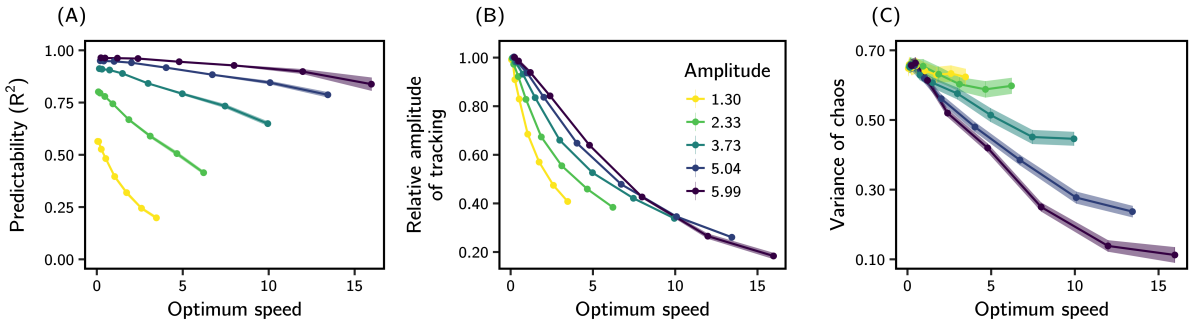

Fig. S8. Linear regression of phenotype on the moving optimum against the average speed of optimum oscillation. The average speed of optimum oscillation (calculated from eq. (2) of the main text as $4\|\mathbf{A}\|/T$) is higher for conditions of short period and high amplitude of oscillations. Predictability, relative amplitude of tracking and variance of chaos were measured as in Fig. 4 of the main text. We show the average (lines and points) and standard error (shading) over 100 simulations for each combination of amplitude and period of optimum oscillation.

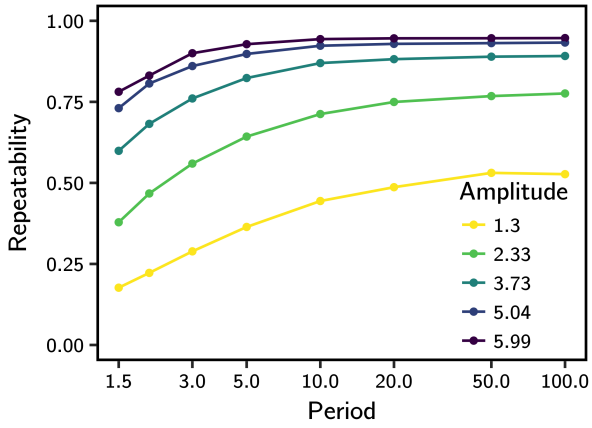

Fig. S9. The repeatability of chaotic trajectories. The ratio of the variance through time of the mean trajectory (mean phenotype averaged across replicates) to the total variance of trajectories (across time and replicates) is shown for each condition of environmental oscillation. We used univariate phenotypic values obtained by scalar projections of the trajectories on the direction of optimum oscillation. The pattern observed is much similar to that of the predictability measured by the R^2 of the linear regression of the phenotype on the optimum (Fig. 4 in the main text). Repeatability differs from our measure of predictability because it does not rely on knowledge of the optimal phenotype.

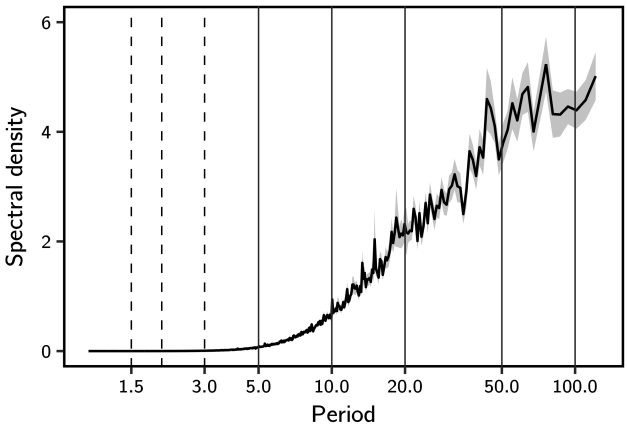

Fig. S10. The average spectral density of evolutionary trajectories in constant environment describes the typical range of periods at which the phenotype oscillates. Among all explored values of period of optimum oscillation (vertical lines) those that led to reduction in the proportion of chaos in relation to the constant environment (as seen in Figure 2, and here marked by vertical dashed lines) are much shorter than the typical oscillations of the system in constant environment. The mean spectral density (solid wiggly line) and its associated standard error of the mean (shading) were calculated based on the 250 trajectories run in constant environment for $d = 70$. The spectrum was calculated as described in the main text, for the projection of the phenotypic vector along the diagonal of the phenotype space.